Protoplasma (1994) 177: 108–122

PROTOPLASMA

Polyanion-mediated mineralization – assembly and reorganization of acidic polysaccharides in the Golgi system of a coccolithophorid alga during mineral deposition

Mary E. Marsh *

Department of Biological Chemistry, Dental Branch, The University of Texas, Houston Health Science Center, Houston, Texas

Received June 26, 1993
Accepted October 6, 1993

Summary. Immunolocalization of two highly acidic polysaccharides (PS-1 and PS-2) in a calcifying alga *Pleurochrysis carterae* is described throughout the mineralization process, from before crystal nucleation through the cessation of crystal growth. This unicellular coccolithophorid alga is a useful model for mineralization because it produces calcified scales known as coccoliths in homogeneous cell culture. PS-1 and PS-2 were localized in the crystal coats of mature coccoliths and in electron dense Golgi particles. The polyanions are synthesized in medial Golgi cisternae and co-aggregate with calcium ions into discrete 25 nm particles. Particle-laden vesicles bud from cisternal margins and fuse with a coccolith-forming saccule containing an organic oval-shaped scale which forms the base of the future coccolith. The particles are localized on the base before the onset of mineral deposition and are present in the coccolith saccule throughout the period of crystal ($CaCO_3$) nucleation and growth. During the final phase of coccolith formation, the particles disappear, and the mature crystals acquire an amorphous coat containing PS-1 and PS-2 polysaccharides which remain with the mineral phase after the coccoliths are extruded from the cell. Postulated mechanisms of polyanion-mediated mineralization are reviewed and their relevance to the calcification of coccoliths is addressed.

Keywords: Algae; Calcium; Coccolithophorids; Golgi; Mineralization; Polyanions; Polysaccharides.

Abbreviations: PS-1 polysaccharide one; PS-2 polysaccharide two; BSA bovine serum albumin; SDS sodium dodecyl sulfate; MES 2-(N-morpholino)-ethanesulfonic acid; EDTA ethylenediaminetetraacetic acid; DHA 3-deoxy-lyxo-2-heptulosaric acid; TCA trichloroacetic acid.

Introduction

Highly acidic macromolecules are postulated intermediates in tissue mineralization, because they sequester large numbers of calcium ions and occur in high concentrations at mineralizing foci in distantly related organisms (Lee et al. 1977, Stetler-Stevenson and Veis 1987, Marsh 1989, Marsh and Sass 1983, Marsh et al. 1992). Phosphoprotein polyanions are intimately associated with mineral phases in bivalve molluscs and vertebrate dentin. The dentin phosphoproteins, also known as phosphophoryns, are aspartic acid- and phosphoserine-rich proteins secreted by odontoblasts at the mineralization front (Dimuzio and Veis 1978 a, b). Similar phosphoproteins, in the form of 40 nm calcium-rich particles, accumulate at the shell mineralization front in some bivalve molluscs (Marsh and Sass 1984, Marsh 1986). Less acidic phosphorylated sialoproteins are intimately associated with the mineral phase of vertebrate bone (McKee et al. 1992, Glimcher 1989). The mineralizing function of phosphoprotein polyanions is poorly understood, largely due to the complexity of calcifying systems in metazoan organisms.

The mineral-associated polyanions of the coccolithophorid alga *Pleurochrysis carterae* are acidic polysaccharides (Marsh et al. 1992). The most abundant polyanion (PS-2) has an unusual structure, a repeating sequence consisting of D-glucuronic, *meso*-tartaric, and glyoxylic acid residues (Fig. 1). The tartrate and glyoxylate residues are probably introduced in a post-polymerization process by oxidative cleavage of C 2–C 3 bonds in alternate residues of a nascent polyuronide. With a net charge of -4 electron units per disaccharide repeat, PS-2 is the most acidic mineral-as-

* Correspondence and reprints: Department of Biological Chemistry, The University of Texas, Houston Health Science Center, Dental Branch, P.O. Box 20068, Houston, TX 77225, U.S.A.

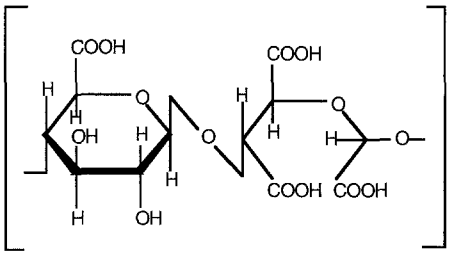

Fig. 1. Structure of the mineral-associated algal polysaccharide PS-2

sociated polyanion yet described. Another algal polyanion, PS-1, has a more conventional composition. It is a polyuronide with a glucuronic/galacturonic acid ratio of 1 : 3 and contains small amounts of uncharged glycosyl residues. PS-1 and PS-2 represent about 22 and 77%, respectively, of the mineral-associated polyanion fraction in *P. carterae*. Since this alga is easily grown in homogeneous cell culture, its glycosidic polyanions should be more amenable to detailed functional studies than the phosphoprotein polyanions of metazoan organisms.

The ultrastructure of *P. carterae* has been described by Manton and Leedale (1969), Manton and Peterfi (1969), Pienaar (1969, 1976), Outka and Williams (1971), and van der Wal et al. (1983 a). The cells are surrounded by a coccosphere consisting of a layer of mineralized scales called coccoliths and several underlying layers of non-mineralized scales (Figs. 2 and 3). The coccoliths are organic oval-shaped scales (bases) with a rim of $CaCO_3$ crystals. Figure 2, adapted from van der Wal et al. (1983 a), gives a cross-sectional model of coccolith formation. Unmineralized bases and clusters of 25 nm particles (called coccolithosomes in Outka and Williams 1971) are intermediate structures in coccolith formation and are easily distinguished in the Golgi system. The particles are heavily stained with lead salts and periodate/silver indicating that they are negatively charged carbohydrate-rich structures (van der Wal et al. 1983 a). They also have a 6 M calcium content as estimated by electron probe microanalysis (van der Wal et al. 1983 b).

The particles are initially observed at the dilated ends of medial Golgi cisternae (Fig. 2). Particle-containing vesicles released from this site migrate distally through the cytoplasm. Bases develop in more distal cisternae and upon completion are also released in vesicles. Particle-containing vesicles fuse with the rim of base-containing vesicles to form the coccolith saccule. Continual addition of particle-laden vesicles to the coccolith saccule produces long peripheral extensions. Deposition of $CaCO_3$ crystals on the rim of the base is observed after fusion of particle- and base-containing vesicles. Particles are present throughout the period of crystal growth. After apparent cessation of mineralization, the saccule becomes swollen, the particles and peripheral extensions disappear, and the coccolith is extruded. At some point during formation, the coccolith crystals acquire an amorphous carbohydrate-rich coat which persists on the external coccoliths. Outka and Williams (1971) postulated that the particles are carriers of the organic material surrounding the coccolith crystals, and van der Wal et al. (1983 b) proposed that they are also carriers of the calcium ions in the mineral phase. In an effort to clarify polyanion function, the association of PS-1 and PS-2 with the particles and mineral phase is described during all phases of mineralization, from before crystal nucleation through the cessation of crystal growth.

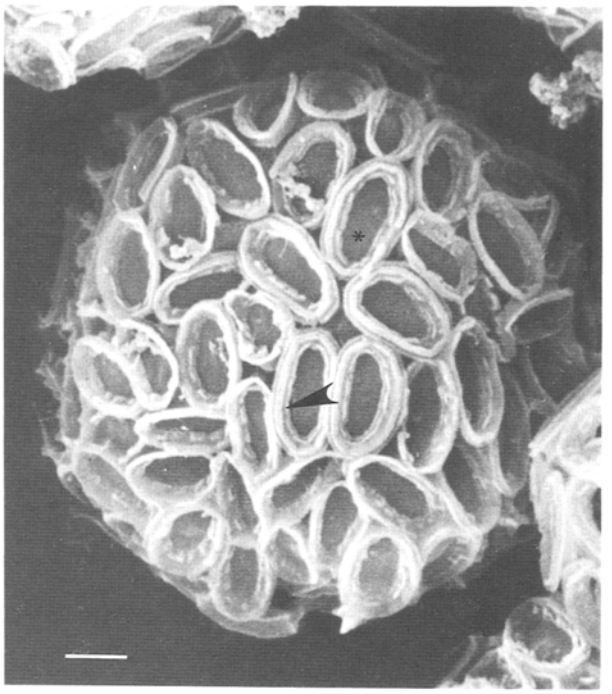

Fig. 2. Scanning electron micrograph of a *P. carterae* cell showing the mineralized scales of the coccosphere. These scales, called coccoliths, consist of organic oval-shaped bases (*) with rims of $CaCO_3$ crystals (arrowhead). An organic coat surrounding the crystals cannot be distinguished in scanning images. Cells were fixed 30 min in 1% OsO_4 in sea water, dehydrated in ethanol, dried from Peldri II (Ted Pella, Inc, Redding, CA) and examined in a JEOL JSM 820 electron microscope. Bar: 1.0 µm

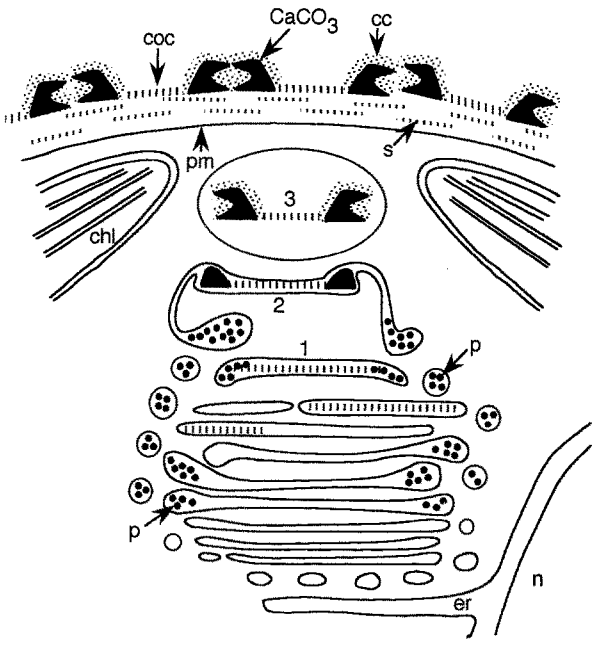

Fig. 3. Cross-sectional model of coccolith formation in *P. carterae* adapted from van der Wal et al. (1983 a). Calcium-rich particles (*p*) and coccolith bases (represented by hatch marks) are formed in distinct Golgi cisternae and released in vesicles. Subsequently the particle- and base-containing vesicles fuse to form coccolith saccules. Three stages of coccolith formation are illustrated. In stage 1 (*1*) the particles are distributed around the rim of the base but no mineral ($CaCO_3$) is present. During stage 2 (*2*) mineral is deposited on the rim of the base, and the particles are generally observed in the dilated ends of slender extensions connected peripherally to the coccolith saccule. Less frequently, particles are also observed surrounding the growing crystals (Fig. 14). At stage 3 (*3*) the coccolith is mature, the saccule is swollen, and the peripheral extensions and particles have disappeared. In this study the organic crystal coats (*cc*) were first observed at stage 3 just prior to extrusion of the coccolith through the plasma membrane (*pm*). Unmineralized scales (*s*), which are smaller than coccolith bases, are also formed in the Golgi apparatus, but are extruded into the coccosphere without interacting with the particles or acquiring a mineral rim. *n* Nucleus, *er* endoplasmic reticulum, *chl* chloroplasts, *coc* extracellular coccoliths

Materials and methods

Antibody preparation and characterization

PS-1 and PS-2 were isolated from *P. carterae* coccoliths as previously described (Marsh et al. 1992). For antiserum production, PS-1 (2.3 mg) was covalently cross-linked to an equal amount of bovine serum albumin (BSA) by reaction with 40 mmoles of 1-ethyl-3-(3-dimethylaminopropyl) carbodiimide in 0.75 ml of 0.2 M MES (2-(N-morpholino)-ethanesulfonic acid), pH 4.75, at room temperature for 24 h and dialyzed sequentially against 50 mM NaCl and water. The conjugate (0.4 mg/dose) was mixed with complete Freund's adjuvant and injected subcutaneously into rabbits at Bethyl Laboratories (Montgomery, TX). Two subsequent boosters were administered at two-week intervals. Antiserum to PS-2 was produced in the same manner except that PS-2 was ionically cross-linked to an equivalent amount of methylated BSA (Sigma Chemical Co., St. Louis, MO) as described by Vreeland (1972). Antibodies were affinity purified on PS-1- and PS-2-conjugated resins prepared from AH-Sepharose 4B (Pharmacia, Uppsala, Sweden) as recommended by the manufacturer.

Sodium dodecyl sulfate (SDS) polyacrylamide gel electrophoresis was performed on 12.5% gels, 0.75 mm thick, in the Laemmli (1970) system. Polysaccharide bands were visualized with Stains All (Green et al. 1973). Molecules were electrotransferred to positively charged nylon membranes (Zeta-Probe; Bio-Rad, Hercules, CA) with a semi-dry system (Hoefer, San Francisco, CA) for 30 min at 100 mA as described by Kyhse-Andersen (1984) except that methanol was omitted from the transfer buffer. Membranes were blocked over night with 5% dry milk in calcium buffer (0.1 M NaCl, 20 mM Tris, pH 7.5, 2 mM $CaCl_2$) and immunostained by sequential treatment with affinity-purified anti-polysaccharide antibodies (0.28 µg/ml) and horseradish peroxidase-conjugated goat anti-rabbit IgG (Bio-Rad; diluted 1 : 3000) in calcium buffer containing 1% dry milk for 1 h. Bands were visualized with 0.5% 4-chloro-1-naphthol, 0.05% hydrogen peroxide, and 17% methanol in calcium buffer. PS-1 does not bind tightly to Zeta Probe, nitrocellulose, Immobilon, or DEAE membranes; however, PS-2 binds strongly to Zeta Probe in the presence of calcium ions.

Ultrastructural localization

The COCCO II strain of *P. carterae* (formerly *Hymenomonas carterae* and *Cricosphaera carterae*) was obtained from the Bigalow Laboratory (West Boothbay Harbor, ME) and one-liter cultures were grown as described (Marsh et al. 1992). Log phase cultures (about 100 cells/ml) were collected by centrifugation at 600 g for 2 min. Cells were fixed 30 min in 3% paraformaldehyde in synthetic sea water (Lyman and Fleming 1940) at pH 8.5 and postfixed 30 min in 1% OsO_4 in the same buffer. After osmification some preparations were demineralized by suspending the cells in 50 mM sodium acetate, pH 4.0, for 1.5 min, followed by alkalination with 3.0 M Tris, pH 8.8. Mineralized and demineralized cells were embedded in 1.5% agarose, dehydrated with ethanol, and embedded in either Epon (LX-112; Ladd, Burlington, VT) or LR White (medium grade; Fullam, Lantham, NY). Both resins were polymerized overnight at 60 °C.

Thin sections on Formvar-coated nickel grids were treated 30 min with affinity-purified anti-PS-1 (0.55 µg/ml) or anti-PS-2 (0.90 µg/ml) in 0.2 M NaCl, 40 mM Tris, pH 7.5, 4 mM $CaCl_2$ containing 1% gelatin followed by 30 min with goat anti-rabbit IgG conjugated with 10 nm colloidal gold particles (Amersham, Arlington Heights, IL) diluted 1 : 10 with the same medium. Sections were stained sequentially with 1% aqueous uranyl acetate and 0.4% lead citrate in 1 N NaOH. In control experiments, polysaccharide antibodies were omitted or replaced with preimmune sera. Anti-PS-1 binds only to LR White sections, and anti-PS-2 binds only to Epon sections.

Biochemical analyses

Calcium-binding measurements were performed at room temperature and pH 8.3. $^{45}CaCl_2$ of known specific activity was added to polysaccharide solutions, and ultrafiltrates were collected by centrifugation for 20 min at 2000 g in Millipore micropartition units (UFC3LGC00) equipped with low-binding, 10,000 nominal molecular weight exclusion membranes. Polysaccharide-bound calcium was determined as the difference in total and free (ultrafilterable) calcium ion concentrations. Uronic acid was measured by the phenyl

phenol assay of Blumenkrantz and Asboe-Hansen (1973). Glucuronic acid concentration (X) was determined from the relationship

$$X = C/(ar + b)$$

where C is the absorbance of the polysaccharide solution in the phenyl phenol assay, a and b are the molar absorptivity of galacturonic and glucuronic acid, respectively, and r is the galacturonate/glucuronate ratio in the polysaccharide. The galacturonate concentration (Y) is rX. In PS-1 the total carboxyl concentration is X + Y. In PS-2 the total carboxyl concentration is 4X + Y, because for each glucuronate residue there is one tartrate residue and one glyoxylate residue (Marsh et al. 1992). Coccolith calcium was extracted with EDTA (Marsh et al. 1992) and measured by atomic absorption spectrometry.

Results

Characterization of anti-polysaccharide IgGs

The PS-2 antigen-antibody interaction requires calcium ions. Anti-PS-2 was retained on Sepharose-conjugated PS-2 columns in calcium containing buffers and was eluted with similar buffers containing excess EDTA (Fig. 4 A). About 81 µg of anti-PS-2 antibody were obtained per ml of immune serum. The PS-1 antigen-antibody interaction is independent of calcium ions. Anti-PS-1, which bound to PS-1-conjugated Sepharose in calcium-containing buffers, was retained in the presence of excess EDTA and was eluted with acidic buffers (Fig. 4 B). About 50 µg of anti-PS-1 antibody were obtained per ml of immune serum.

The PS-2 polysaccharides migrate as a ladder of discrete bands on polyacrylamide gels (Fig. 5 a), because their degree of polymerization is highly variable. PS-1 polysaccharides have a narrow range of molecular weights and migrate in a relatively tight band. PS-1 and PS-2 bands can be electrotransferred to Zeta Probe and visualized with ruthenium red (not shown) as described by Charak et al. (1990). However, PS-1 dissociates from Zeta Probe and all other membranes tested when equilibrated with buffer for 1 h. Therefore, direct visualization of PS-1 with anti-PS-1 antibody on Western blots is not possible. In contrast, PS-2 binds tightly to Zeta Probe when incubated in calcium-containing buffers. Membrane-bound PS-2 reacts with anti-PS-2 but not with anti-PS-1 antibodies (Fig. 5 b).

PS-1 and PS-2 co-aggregate in the presence of calcium ions (Marsh et al. 1992), most likely via formation of Ca^{2+} cross-bridges between negatively charged polyanion chains. In a similar manner PS-2 bands immobilized on Zeta Probe bind PS-1 when incubated in solutions containing PS-1 and calcium ions. Thus when membranes containing immobilized PS-2 bands are preequilibrated with excess PS-1 in the presence of Ca^{2+}, the ladder of PS-2 bands immunostains strongly

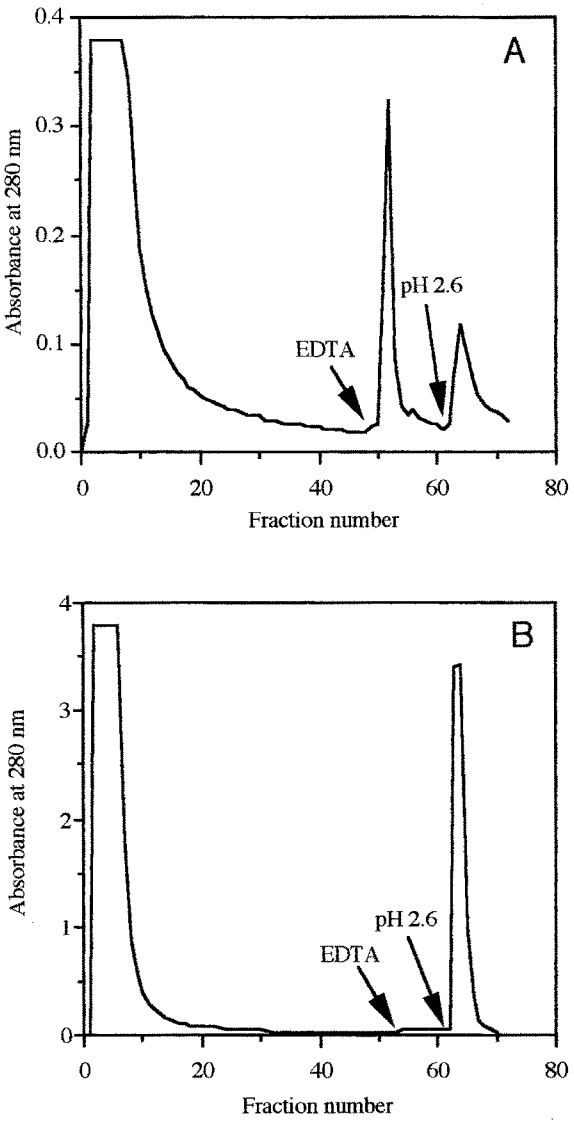

Fig. 4. **A** Chromatography of anti-PS-2 serum on PS-2-conjugated Sepharose 4 B. 10 ml of serum were dialyzed versus calcium buffer (4 mM $CaCl_2$, 200 mM NaCl, 40 mM Tris, pH 7.5) and applied to a 1.0 × 5.0 cm column of resin equilibrated with the same buffer. The column was washed with 150 ml of calcium buffer, and 3.0 ml fractions were collected at a flow rate of 60 ml/h. Then the column was successively eluted with 8 mM EDTA in calcium buffer and 0.2 M glycine, pH 2.6 (arrows). Fractions (1.5 ml) were collected at the same flow rate. The EDTA peak contained all the anti-PS-2 activity. The pH 2.6 peak contained no activity. **B** Chromatography of anti-PS-1 serum on PS-1-conjugated Sepharose 4 B. Conditions are as described above. Little activity was associated with the EDTA fractions. The pH 2.6 peak contained the bulk of the anti-PS-1 activity and a lot of extraneous protein. The latter was removed by chromatography of the acidic fraction on PS-2-conjugated Sepharose in calcium buffer. The flow-through fraction from the PS-2 column contained all the anti-PS-1 activity while 95% of the protein was retained on the column

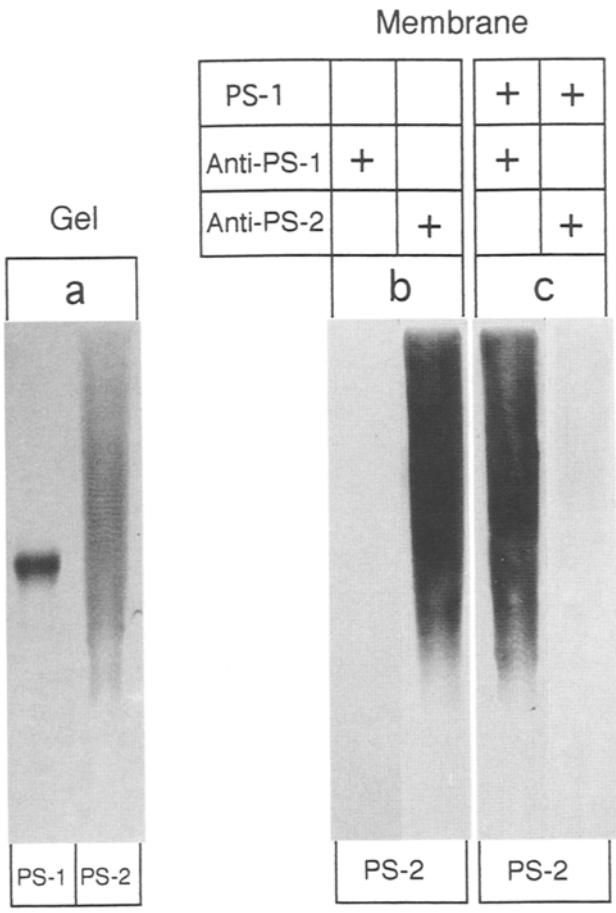

Fig. 5. **a** SDS-polyacrylamide gel of PS-1 (7 µg) and PS-2 (12 µg) stained with Stains-All. **b** PS-2 (12 µg) transferred to Zeta Probe and immunostained with anti-PS-1 or anti-PS-2. **c** Similar to **b** except that the membrane was preequilibrated overnight with 40 µg of PS-1 in blocking solution. Membranes were thoroughly rinsed with buffer before immunostaining

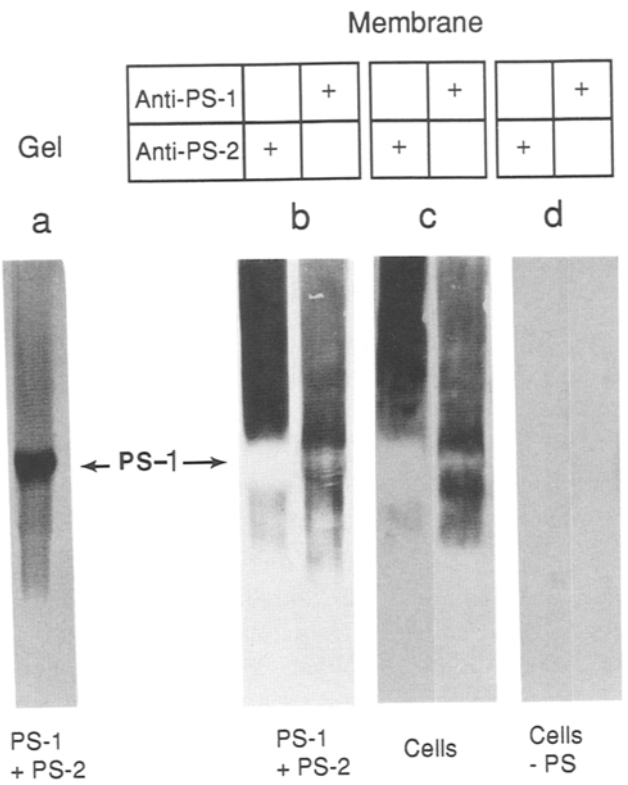

Fig. 6. **a** SDS-polyacrylamide gel of a mixture of PS-1 (7 µg) and PS-2 (12 µg) stained with Stains-All. **b** PS-1 and PS-2 mixture transferred to Zeta Probe and immunostained with anti-PS-1 or anti-PS-2. **c** SDS/EDTA extract of *P. carterae* cells resolved on polyacrylamide gels, transferred to Zeta Probe, and probed with anti-PS-1 or anti-PS-2. Cells (6.5×10^7) were sonicated in 0.5 ml of 0.2 M EDTA, pH 8.3. Then 0.5 ml of SDS solution (4% SDS, 20% glycerol, 10% 2-mercaptoethanol, 0.125 M Tris, pH 6.8) was added and the extract heated 5 min at 100 °C. After centrifugation for 10 min at 14,000 **g**, 25 µl of the supernatant fluid was added to each lane. **d** Same as **c** except that the cells were extracted with 5% TCA to remove the acidic polysaccharides before treatment with SDS/EDTA

Fig. 7. **A** Transmission electron micrograph of isolated coccoliths deposited on a Formvar-coated grid. The dense oval-shaped structures are the $CaCO_3$ rims. The coccolith bases (*) and the organic crystal coats are not distinguishable. The individual crystalline units are easily recognized on one coccolith (arrowhead). Coccoliths were isolated as previously described (Marsh et al. 1992). When the coccolith crystals are dissolved with EDTA, calcium ions and polysaccharides (PS-1 and PS-2) are released in a mole ratio of 6.2 calcium ions per polyanion carboxyl group. **B** Coccoliths oxidized 1 h at 85 °C in 5.25% NaOCl (Clorox), washed with water, and deposited on a Formvar-coated grid. The anvil-shaped unit crystals have dissociated from each other and their organic bases. Based on uronic acid assays, no PS-1 or PS-2 is associated with these crystals. Bars: 0.5 µm

Fig. 8. **A** Grazing section through the coccosphere showing the crystal coats. The coats surround electron lucent areas previously occupied by coccolith crystals lost during sectioning and staining procedures. This Epon section was treated sequentially with rabbit anti-PS-2 and colloidal gold-anti-rabbit IgG. The coats are heavily labeled with gold particles. **B** Similar to **A** except that anti-PS-2 was replaced with preimmune serum. The crystal coats are unlabeled. Coccolith bases (arrow) and nonmineralized scales (arrowhead) are apparent. Bars: 0.5 µm

Fig. 9. **A** Grazing section through the coccosphere showing the crystal coats in an LR White section stained sequentially with rabbit anti-PS-1 and colloidal gold-anti-rabbit IgG. The crystal coats are heavily labeled, but the coccolith base (arrowhead) and the unmineralized scales (arrow) are unlabeled. **B** Similar to **A** except that anti-PS-1 was replaced by preimmune serum. Here the crystal coats are unlabeled. Bars: 0.5 µm

Fig. 10. An Epon section from *P. carterae* cells briefly demineralized before dehydration and embedding. In this section the contours of the unit crystals are well preserved illustrating that the polysaccharide coats surround each individual crystallite. The coats, but not the coccolith base (arrowhead) are labeled by sequential treatment with rabbit anti-PS-2 and colloidal gold-anti-rabbit IgG. Coccoliths are sectioned parallel (*a*) and perpendicular (*b*) to the plane of the base. Bar: 0.5 µm

with anti-PS-1, but very weakly with anti-PS-2 (Fig. 5 c). The latter observation indicates that PS-1 has bound to most of the epitopes recognizable by anti-PS-2. It also shows that anti-PS-2 does not bind to PS-1.

Mixtures of PS-1 and PS-2 resolved on polyacrylamide gels (Fig. 6 a) and transferred to Zeta Probe, show distinctive staining patterns when probed with anti-PS-1 or anti-PS-2 (Fig. 6 b). When equilibrated with anti-PS-1, staining is observed over the entire set of PS-2 bands.

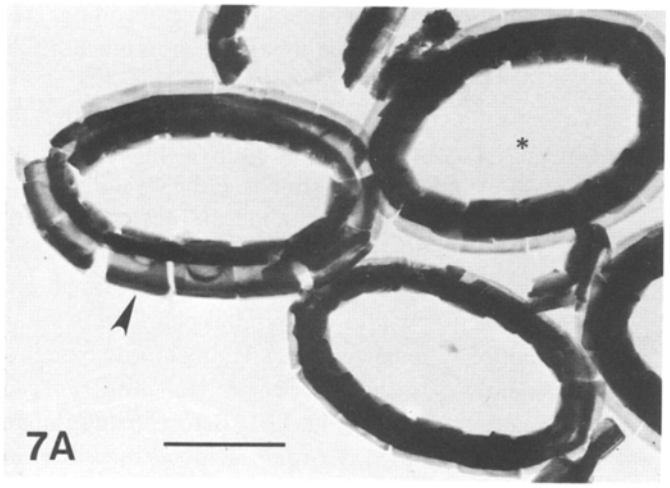

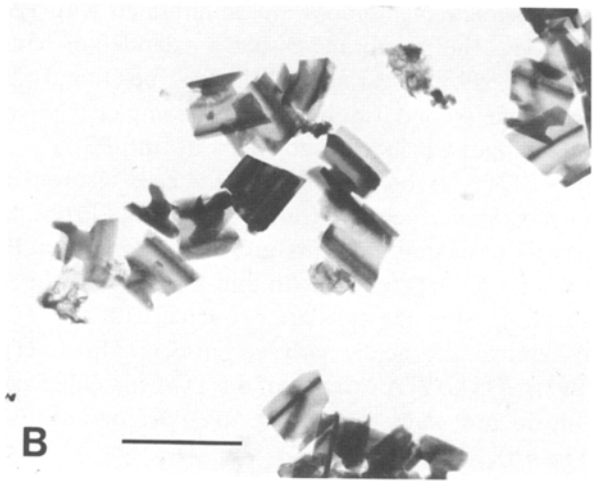

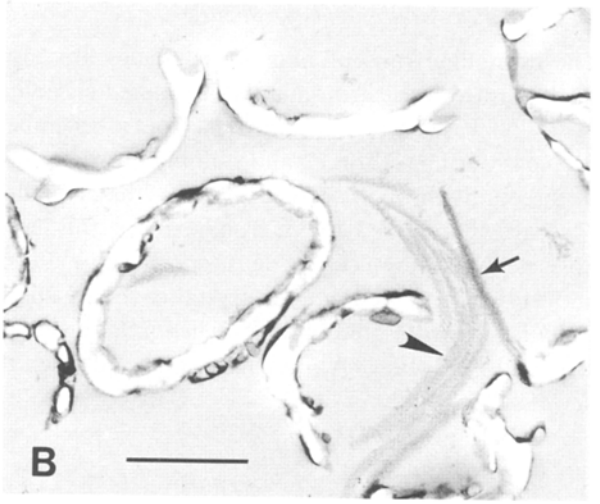

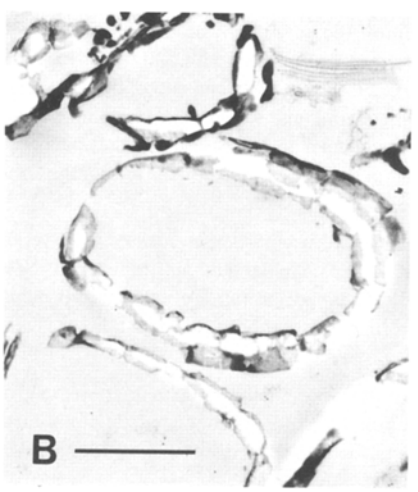

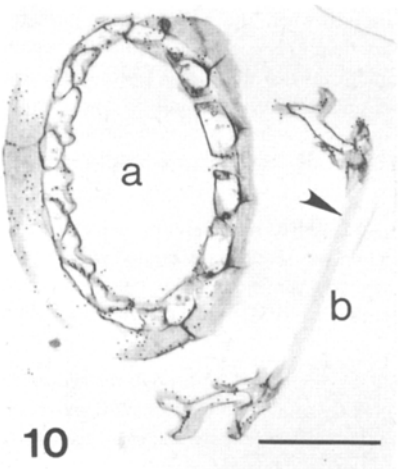

This pattern shows that the PS-1 has dissociated from the membrane and rebound to all of the PS-2 bands. Weaker staining with PS-1 antibody is observed at the center of the PS-1 zone, probably because there is less PS-2 at this site and hence less secondarily bound PS-1. PS-2 bands may be distorted about the PS-1 zone when the polyanions are electrophoresed as a mixture. When similar membranes are equilibrated with PS-2 antibody, the membrane displays a ladder of bands interrupted by a clear zone at the PS-1 position. In the clear zone secondarily bound PS-1 completely covers the epitopes which are recognized by anti-PS-2.

SDS/EDTA extracts of *P. carterae* cells resolved on polyacrylamide gels and transferred to Zeta Probe display patterns similar to mixtures of pure PS-1 and PS-2 when immunostained with anti-PS-1 and anti-PS-2 (Fig. 6 c). After the cells are extracted with 5% TCA to remove the acidic polysaccharides (Marsh et al. 1992), SDS/EDTA extracts of the TCA-insoluble fraction do not react with either anti-PS-1 or anti-PS-2 (Fig. 6 d).

Ultrastructure and immunolocalization

The crystalline rims of mineralized scales are easily distinguished in electron images of isolated coccoliths (Fig. 7 A). However, crystals are lost from resin-embedded cells during sectioning and staining procedures. In thin sections through the coccosphere, the crystalline rims are represented by oval-shaped electron-lucent holes delineated by electron-dense crystal coats (Figs. 8 and 9). In Epon sections, the crystal coats are specifically labeled with gold particles when immunostained with anti-PS-2 (Fig. 8 A), but are not labeled when the antibody is omitted or replaced with preimmune serum (Fig. 8 B). The coats are only weakly reactive with anti-PS-1 in Epon sections (not shown), but are heavily and specifically labeled with the same antibody in LR White sections (Fig. 9 A, B). Hence, both PS-1 and PS-2 are crystal coat components. The intimate relationship between the coats and crystals is apparent in tissue which has been briefly demineralized before embedding. Here the angular contour of the crystalline units is beautifully preserved by their surrounding coats (Fig. 10).

A chemical method was used to determine whether PS-1 and PS-2 occur within the mineral phase since antibody molecules cannot penetrate the crystallites. Hypochlorite oxidation at alkaline pH destroys organic molecules surrounding $CaCO_3$ crystals, but since the crystals per se are not dissolved by this treatment, organic molecules within the mineral phase are resistant to oxidation (Crenshaw 1972). Hypochlorite oxidation of coccoliths dissociated the crystalline units from each other and the bases (Fig. 7 B). Before oxidation the coccoliths contained 5 uronic acid residues per 100 calcium ions; after oxidation uronic acid was not detected (i.e., was less than 1% of the original level). This shows that the uronic acid-rich polyanions PS-1 and PS-2 occur on the crystal surfaces and are not incorporated within the mineral phase.

The calcium-rich electron-dense particles in the Golgi system are heavily and specifically labeled with both anti-PS-1 and anti-PS-2 (Figs. 11 and 12). The particles are initially observed in the dilated margins of medial Golgi cisternae (Fig. 13). Polysaccharide synthesis and co-aggregation probably occurs at this site, since antibody labeling was not observed in more proximal

Fig. 11. **A** Epon section depicting an immature coccolith (*l*) before the onset of mineral deposition (stage 1, Fig. 3). Dense particles are observed where the section passes through the rim of the base (arrowheads). Particles are also observed in a vesicle (*v*) which is probably part of another coccolith saccule. The section was sequentially treated with rabbit anti-PS-2 and colloidal gold-anti-rabbit IgG. Dense particles in both vesicles are labeled. Cytoplasm, nucleus (*n*), chloroplast (*chl*), and coccolith base are unlabeled. **B** Similar to **A** except that the particles are unlabeled because anti-PS-2 was replaced with preimmune serum. The coccolith shown here (*2*) is in the mineralizing stage (stage 2, Fig. 3). It has been sectioned through the rim perpendicular to the base. Note that particles are contained in dilated lobes (arrowheads) at the ends of slender extensions projecting from the peripheral margins of the coccolith saccule. At this stage the coccolith crystals have no coats. Bars: 0.1 μm

Fig. 12. **A** LR White section depicting a large vesicle laden with dense particles. The vesicle is probably part of a coccolith saccule. The section was sequentially treated with rabbit anti-PS-1 and colloidal gold-anti-rabbit IgG. Note that the particles are heavily labeled, and that the cytoplasm, nucleus (*n*), chloroplast (*chl*), and mitochondrion (*m*) are unlabeled. **B** Similar to **A** except that the particles are unlabeled because anti-PS-1 was replaced with preimmune serum. The coccolith rim shown here (*1*) is in a premineralizing stage (stage 1, Fig. 3). Bars: 0.1 μm

Fig. 13. Epon section through the central region of the Golgi stack. Particles are observed within the dilated ends of medial cisternae and in small Golgi-derived vesicles. With careful observation, hatch marks characteristic of an unmineralized scale or coccolith base can be seen in another cisternae (between arrowheads). Only the particles are labeled in this section treated sequentially with rabbit anti-PS-2 and colloidal gold-anti-rabbit IgG. Bar: 0.1 μm

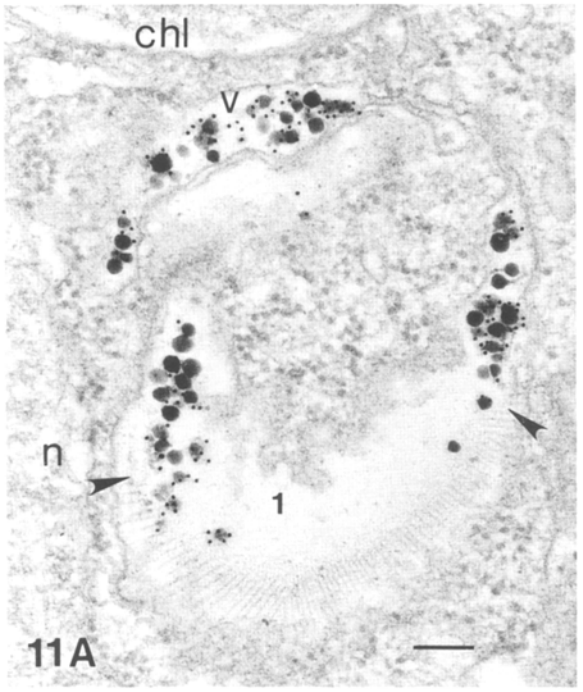
chl
v
n
1
11A

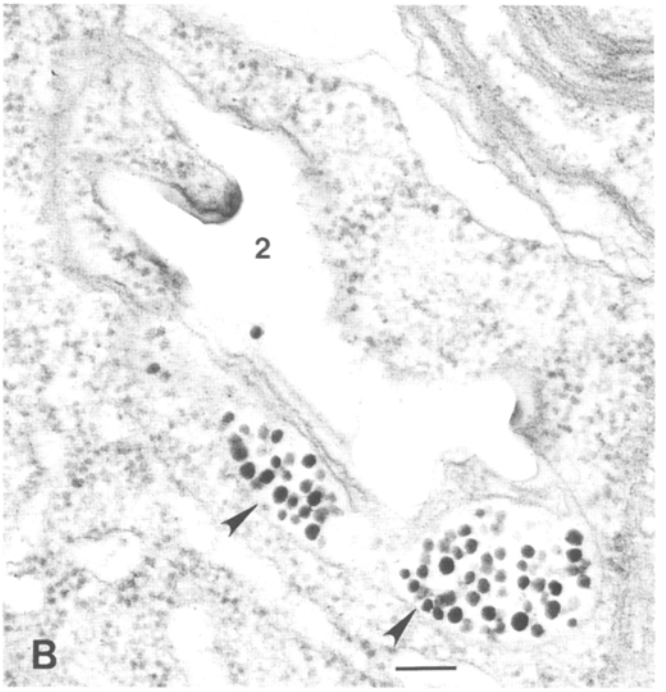
2
B

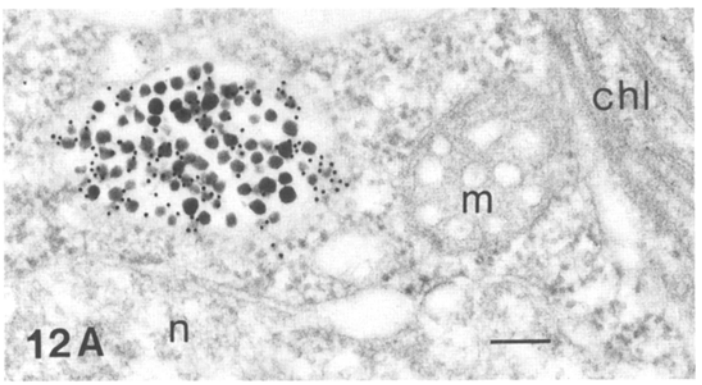
chl
m
n
12A

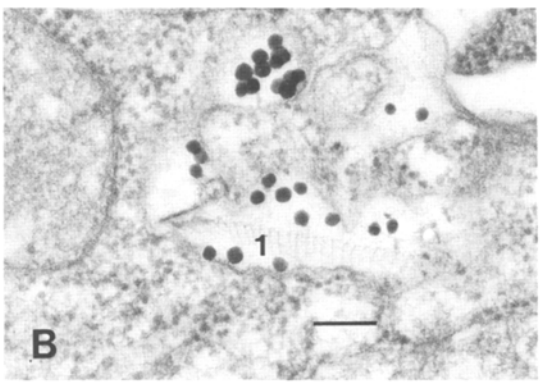
1
B

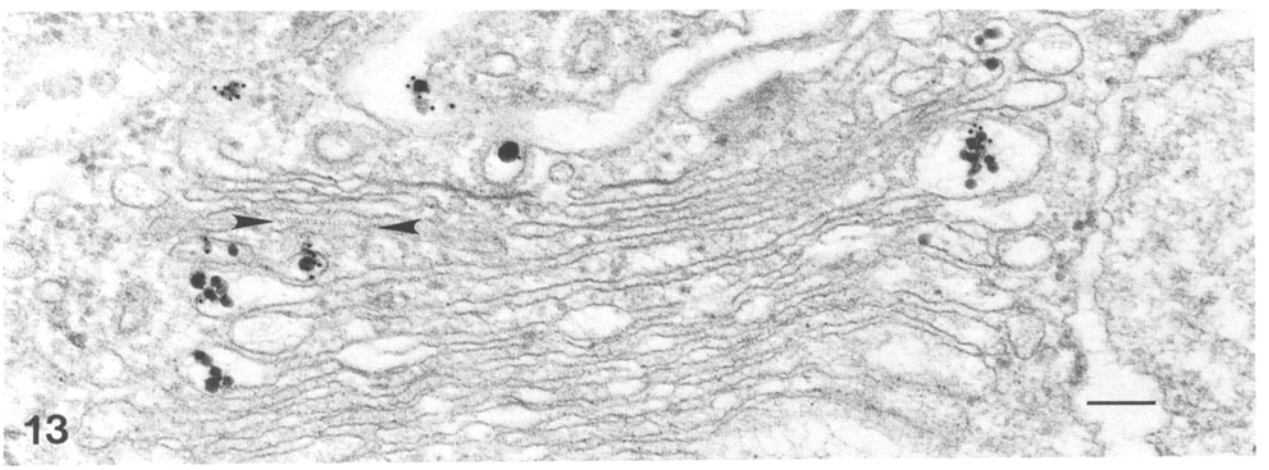
13


2
2
14

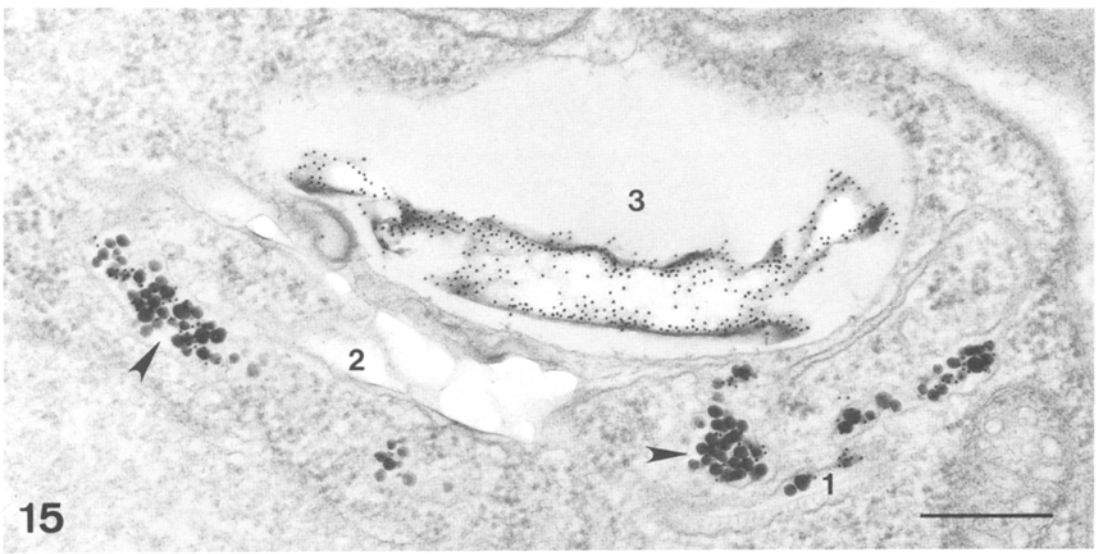
3
2
1
15


3
2
2
16

cisternae. In addition, PS-1 and PS-2 co-aggregate in vitro in the presence of calcium ions (Marsh et al. 1992), indicating that, unless immobilized, PS-1 and PS-2 will co-aggregate with calcium ions in vivo during polymerization if synthesized in the same compartment at a neutral or alkaline pH.

Polysaccharide particles are also observed in Golgi-derived vesicles (Fig. 13) and coccolith-forming saccules. Particles migrate to bases by fusion of particle-containing vesicles with the circumferential margin of base-containing saccules (van der Wal et al. 1983 a). Before the onset of crystal formation, particles in the coccolith saccules are distributed about the rim of the base (Figs. 11 A, 12 B, and 15). This premineralizing phase of coccolith formation is designated stage 1. During crystal growth (stage 2), particles may be observed adhering to the crystal surface (Fig. 14), but more frequently the crystals are bare, and the particles are restricted to the peripheral extensions of the coccolith saccule (Figs. 11 B and 15). The extensions apparently elongate by continual fusion with particle-containing vesicles throughout the mineralization process.

The final phase of coccolith maturation (stage 3) is characterized by saccule dilation with loss of the peripheral extensions (Fig. 15). At this time the crystals also acquire their polysaccharide coat. In contrast to previous reports, in this study crystal coats were never observed before saccule dilation. During crystal growth when the saccule was flattened against the coccolith and possessed lateral extensions, particles were sometimes observed about the crystals but no electron dense coat was present (Figs. 11 B, 14, and 15), and only the occasional gold particle adhered to the crystal surface after immunostaining with polysaccharide antibodies (Figs. 14 and 15). Figure 15 illustrates a mature coccolith with coated crystals in a swollen saccule just prior to extrusion and an underlying immature coccolith with naked crystals in a flattened saccule with peripheral extensions. Note that the coats of the mature coccolith are heavily labeled with immunogold, while no gold particles adhere to the naked crystals of the immature coccolith. Figure 16 shows a demineralized section containing a mature coccolith in a swollen saccule and an immature coccolith in a flattened saccule with extensions. The crystal morphology of the mature coccolith is clearly defined by crystal coats. However, the crystal contours of the immature coccolith are not preserved by crystal coats. Here the position of the crystals is indicated by groups of particles surrounding ill-defined filamentous material on the rim of the base. The source of the filamentous material is unclear; its structure bears no relationship to crystal morphology. Hence, there is no ultrastructural or immunochemical evidence for a PS-1- and PS-2-rich coating on immature coccolith crystals.

Calcium-polysaccharide interactions

Isolated coccoliths contain about 6.2 calcium ions in the mineral phase for each carboxyl group associated with the polyanions in the crystal coats. The amount of calcium sequestered by the polysaccharide particles within the Golgi system is a function of the ionic strength, pH, mineral ion concentration and degree of polymerization of the polyanions. Since the in vivo ionic composition is unknown, calcium-polysaccharide interactions were investigated under a range of conditions (Fig. 17 A, B). PS-1 and PS-2 bind a maximum of 0.45 and 0.38 calcium ions per carboxyl group, respectively, in solutions of low ionic strength at pH 8.3. However, calcium binding decreases with increasing ionic strength. When solutions have a ionic strength

Fig. 14. Epon section treated sequentially with rabbit anti-PS-2 and colloidal gold-anti-rabbit IgG and showing two mineralizing coccoliths. These stage 2 coccoliths (*2*) have particles in contact with the surface of the growing crystals in addition to particles in peripheral extensions (arrowheads). The crystals are uncoated, and few gold particles are observed on the crystal surface except in association with the polysaccharides particles. In this section the gold label on the particles is difficult to discern because both are very dense. Bar: 0.25 μm

Fig. 15. An Epon section similar to Fig. 14 showing the three stages of coccolith formation. At stage 2 (*2*), the crystals are uncoated and do not bind anti-PS-2; the particles are restricted to the peripheral extensions of the coccolith saccule (arrowheads). The stage 3 (*3*) coccolith is in a swollen saccule without particles or extensions. The crystals of this coccolith are coated and heavily labeled with anti-PS-2/colloidal gold. A stage 1 (*1*) coccolith with particles but no crystals is apparent. Bar: 0.25 μm

Fig. 16. Section of a demineralized cell showing coccoliths at stages 2 (*2*) and 3 (*3*). At stage 3 the space previously occupied by the unit crystals is clearly delineated by their surrounding coats. However, at stage 2, the space previously occupied by the growing crystal is not preserved after demineralization. Here the position of the crystals is indicated only by particle clusters on the rim of the base. Within these clusters is a fine filamentous material (arrowheads) which would not be present if this were a premineralizing (stage 1) coccolith. The particles have irregular structures due to the demineralization treatment. The section is not immunostained. Bar: 0.25 μm

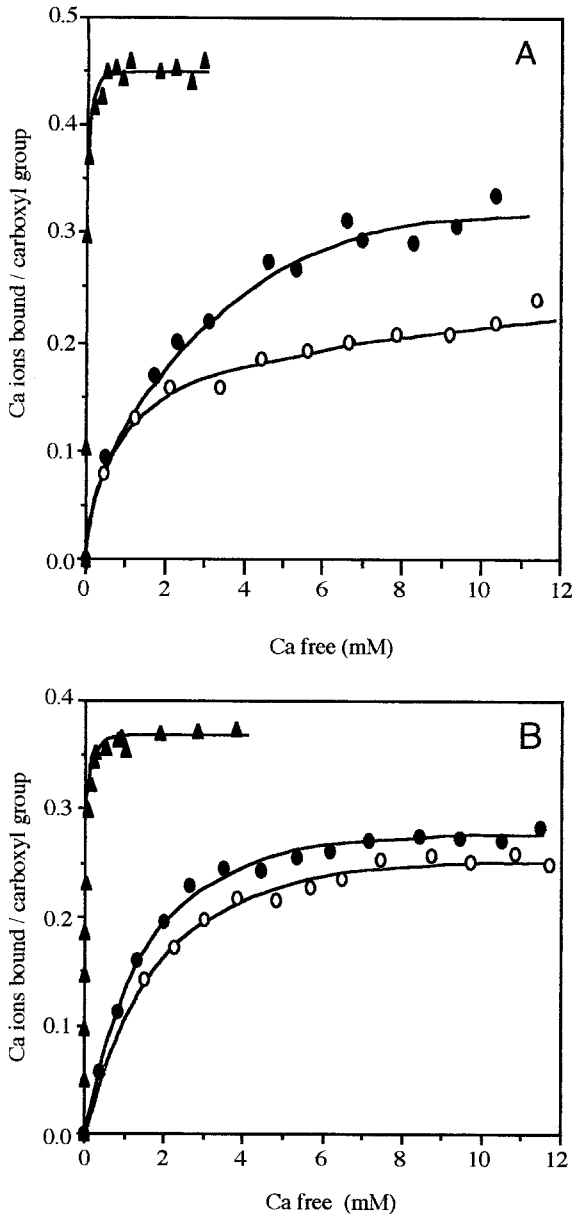

Fig. 17. **A** Titration of PS-1 with $^{45}CaCl_2$. Graph shows the number of calcium ions bound per polysaccharide carboxyl group as a function of the free calcium ion concentration. Buffers are 20 mM Tris, pH 8.3 (▲) and 0.64 M NaCl in 20 mM Tris, pH 8.3 (○, ●). In one study (○), the polysaccharide was titrated with solutions of $^{45}CaCl_2$ and $MgCl_2$ in a mole ratio of 1 : 5.23 similar to the mole ratio observed in sea water. Here the buffer concentration was decreased during titration to maintain a ionic strength of about 0.65 M (also similar to sea water). Polysaccharide solutions contained 1.0–10 mmoles of carboxyl groups per ml, and in this range, bound calcium was independent of polysaccharide concentration (not shown). **B** Titration of PS-2 with $^{45}CaCl_2$. Conditions are as in **A**

and calcium ion concentration similar to sea water (0.648 M and 10 mM, respectively), PS-1 and PS-2 bind only 0.30 and 0.28 calcium ions per carboxyl group, respectively. When solutions are also 52.3 mM in magnesium ions (similar to sea water), the bound Ca^{2+} per carboxyl drops to 0.22 and 0.26 in PS-1 and PS-2, respectively. At high ionic strength the apparent calcium dissociation constant for PS-1 and PS-2 is about 1 mM. Here the apparent dissociation constant is defined as the free calcium concentration at which the level of bound calcium is half of that observed in 10 mM Ca^{2+} (the concentration of calcium ions in sea water). If the average molecular weight of polyanions associated with coccolith mineralization is considerably greater than those isolated from mature coccoliths, then the calcium ion affinities of the former may be somewhat larger than the values given here.

Discussion

Antibody specificities

A circuitous demonstration of PS-1 and PS-2 antibody specificity was required in this study because (1) PS-1 does not bind tightly to any membrane tested, (2) PS-1 binds to membrane-bound PS-2 bands in the presence of calcium ions, and (3) PS-2 bands cover most of the polyacrylamide gel, potentially obscuring other molecular species capable of binding anti-PS-2 on Western blots. However, it is clear that anti-PS-1 binds specifically to PS-1-conjugated Sepharose and PS-1-Ca^{2+}-PS-2 conjugates immobilized on Zeta Probe. Anti-PS-2 specifically binds to PS-2-conjugated Sepharose and PS-2 immobilized on Zeta Probe. Anti-PS-1 and anti-PS-2 do not bind TCA-insoluble extracts of *P. carterae* cells which contain no acidic polysaccharides. Hence, anti-PS-1 and anti-PS-2 are probably monospecific antibodies, binding only PS-1 and PS-2, respectively.
PS-2/anti-PS-2 and PS-1/anti-PS-1 interactions are different. The former is calcium ion-dependent and the latter is not. In addition, anti-PS-1 IgG binds to *P. carterae* cells embedded in LR White resin but not in Epon. Conversely anti-PS-2 IgG binds to cells embedded in Epon but not in LR White.

Ultrastructure and immunolocalization

PS-1 and PS-2 are synthesized within the dilated margins of medial Golgi cisternae and co-aggregate into discrete particles. The polyanion particles migrate to the coccolith saccule via Golgi-derived vesicles and are localized on the rim of the coccolith base before the onset of mineral deposition (stage 1). During $CaCO_3$ deposition (stage 2), the polyanions in their particulate form may be observed adhering to the crystal surface, but more frequently, the crystals are bare, and the

particles are restricted to the peripheral extensions of the coccolith saccules (Fig. 3). During the final phase of coccolith formation (stage 3), the particles disappear, and the mature crystals acquire on amorphous coat containing PS-1 and PS-2 polysaccharides which remains with the mineral phase after the coccoliths are extruded from the cell. Only the crystal coats of mature coccoliths and the dense particles in the Golgi system contain PS-1 and PS-2 polysaccharides. The polyanions are not incorporated within the mineral phase.

This study shows that the acquisition of the crystal coats is a postmineralization process and differs from a previous report (van der Wal et al. 1983 a) indicating that crystal growth and formation of crystal coats are simultaneous processes. In that study carbohydrate material was observed on the surface of immature crystals based on a silver proteinate assay. Since the saccule membrane is closely apposed to the surface of immature crystals, the glycosyl residues may have been associated with membrane glycoconjugates rather than a true crystal coat.

Mineralizing function of polyanions

Highly acidic polyanions are postulated intermediates in tissue calcification, because they sequester large numbers of calcium ions and are associated with mineralized structures in distantly related organisms. This is the first study which localizes specific polyanions during all phases of mineralization, from before crystal nucleation to the cessation of crystal growth. Therefore it is worthwhile reviewing postulated mechanisms of polyanion-mediated mineralization and considering their relevance to the mineralization of coccoliths.

Polyanions may function as intermediate calcium carriers (van der Wal et al. 1983 b, Dimuzio and Veis 1978 b, Marsh and Sass 1984). According to this hypothesis, calcium ions initially sequestered by the polyanions are transferred to the mineral phase. Transfer begins with dissociation of calcium from the polyanion and may be achieved through acidification, chelation of calcium by other agents, or depolymerization of the polyanion. At mineralizing foci, the former are ineffective, since calcium minerals are acid-soluble and chelated calcium is unavailable for mineral precipitation. However, polyanion degradation is effective; it considerably increases the free calcium ion activity since calcium dissociation constants are much greater for simple anions than for large polyanions.

Consistent with the carrier hypothesis, the algal polyanions are charged with calcium ions before deposition of $CaCO_3$, i.e., electron microprobe analyses show the polyanion particles are about 6 M in calcium ions (van der Wal et al. 1983 b). The appearance of the polyanion particles at the mineralization front just prior to the onset of calcium deposition is also in agreement with the carrier hypothesis, and the absence or intermittent presence of polyanions at crystal surfaces during growth is consistent with a rapid degradation of polyanions at that site. As the polyanions depolymerize, calcium would be precipitated as $CaCO_3$, while the organic anions (polyanion fragments) could be taken up by the cytoplasm (Fig. 18 A). According to the carrier hypothesis, crystals would continue to grow as long as polyanions and degrading enzymes were available. The reappearance of polyanions at the crystal surface in a different organizational form at the end

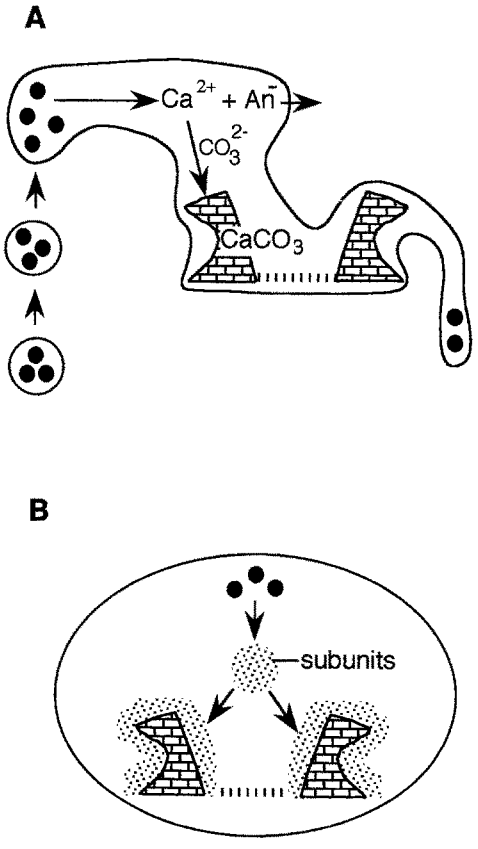

Fig. 18. A Scheme showing a postulated mechanism for calcium ion accumulation during coccolith mineralization. Vesicles bearing calcium-polyanion particles fuse with a mineralizing coccolith saccule. At this site the polyanion is degraded into small anions (An^-) and free Ca^{2+} ions. The calcium ions are precipitated as $CaCO_3$ on the coccolith rim, and the anions are taken up by the cytoplasm. **B** Scheme showing postulated mechanism for crystal coat formation. After swelling of the coccolith saccule, the residual particles disaggregate into smaller subunits. The subunits bind to the crystal surface forming a rather uniform amorphous coat

of mineral growth is not as readily explained. Perhaps dissociation of the particles into subunit structures as observed by Outka and Williams (1971) is an initial stage in polyanion degradation. After swelling of the coccolith saccule, degradation of residual polyanion particles may be halted at the subunit stage, resulting in cessation of mineralization and binding of subunits to crystal surfaces (Fig. 18 B).

Mineralizing polyanions may also function as calcium buffers similar to calsequestrin and calreticulin in the endomembrane systems of muscle and nonmuscle cells, respectively (Milner et al. 1992). Consistent with this theory, PS-1 and PS-2 are capable of buffering calcium in Golgi vesicles, since they sequester large numbers of calcium ions with a dissociation constant of about 1 mM at high ionic strength. However, if polyanions serve only as a calcium buffer, they need not be degraded during mineralization.

Polyanions may also regulate mineralization through nucleation and/or inhibition mechanisms. Many in vitro studies have shown that dissolved polyanions inhibit the precipitation and growth of calcium minerals by sequestering small nuclei and binding to crystal faces (reviewed in Wheeler and Sikes 1989). Conversely polyanions facilitate the nucleation of calcium minerals when immobilized on a solid substrate (Linde et al. 1989), theoretically through a ionotropic or stereochemical mechanism (Crenshaw 1982, Addadi and Weiner 1985). Consistent with a nucleation/inhibition function, the algal polyanions are located on the rim of the coccolith base when $CaCO_3$ formation is initiated, and the crystal surfaces are covered with a polyanion coat when mineralization ceases. However, it is unclear whether mineralization ceases because the crystals become covered with polyanions, or whether polyanions are added to the crystals after mineralization has ceased.

Even though the algal polysaccharides are likely to inhibit and facilitate $CaCO_3$ deposition in vitro similar to other polyanions, it would be difficult to demonstrate that they have a similar function in vivo. Immunocytochemical and ultrastructural studies do not have sufficient resolution to establish intermolecular distances between polyanion domains and calcium carbonate ion clusters when the first stable nuclei are formed. The acquisition of a polyanion coat is an unlikely mechanism for terminating or inhibiting crystal growth in *P. carterae*. If immobilized polyanions are efficient nucleators, then mineral should overgrow the coats when the calcium carbonate ion product exceeds the solubility product. In a similar manner $CaCO_3$ overgrows the organic membrane covering earlier crystals during successive cycles of mineralization in the septal nacre of *Nautilus pompilius* (Crenshaw and Ristedt 1976).

There is compelling evidence that polyanions have a central role in coccolith mineralization, but whether they function as calcium carriers and/or regulators of crystal nucleation and growth is unclear. *P. carterae* should be a particularly useful model for testing the carrier hypothesis but has no apparent advantage over other systems as an experimental model for testing nucleation/inhibition theories. The carrier hypothesis can be tested by measuring the rate of polyanion turnover in pulse-labeling experiments. In vivo PS-1 and PS-2 probably sequester one calcium ion per 2–4 carboxyl groups depending on the ionic strength and composition inside Golgi vesicles, while mature coccoliths contain about 6.2 calcium ions for each polyanion carboxyl group in the crystal coats. Thus if all of the coccolith calcium is carried by polyanion particles, then most of the polyanion fraction must be degraded during mineral deposition. Based on the numbers above, 92–96% of the polyanions synthesized should be turned over during mineralization while the remaining 4–8% are assembled into crystal coats. If the algal polyanions turnover, then examination of polyanion metabolism in more complex systems during mineral deposition should be worthwhile. This is particularly true of the highly phosphorylated proteins of tooth dentin and molluscan shells.

Other algal cultures

The mineralizing saccules of another coccolithophorid alga *Emiliania huxleyi* do not contain electron dense particles; however, a highly complex polysaccharide with relatively few acidic residues is associated with the coccoliths (de Vrind-de Jong et al. 1986). This polysaccharide is unrelated to the *P. carterae* polyanions, and its function is unknown. The coccolith saccule of *E. huxleyi* is attached to a reticular body (a system of anastomozing tubules) during mineral deposition (van der Wal et al. 1983 c, Westbroek et al. 1986). The vast membrane surface of this structure may provide a high concentration of calcium pumps to facilitate rapid accumulation and deposition of calcium ions. The apparent absence of highly acidic polyanions suggests that the coccolith-forming saccules are capable of acquiring a high enough calcium ion concentration through membrane pumps alone to drive the precipitation of $CaCO_3$. A unicellular green alga, *Mesostigma viride*, produces

elaborate basket-shaped scales which are mineralized with calcium and phosphate ions (Domozych et al. 1991). The amount and crystallographic form of the mineral phase has not been determined. The basket scales are produced in the peripheral zone of medial-trans Golgi cisternae, and appear to be mineralized by vesicles transporting calcium to the cisternal loci from large calcium-laden vacuoles (Domozych et al. 1992). About 24% of the scale mass is carbohydrate, and the unusual dicarboxylic acid sugar, 3-deoxy-lyxo-2-heptulosaric acid (DHA), represents about 40% of the glycosyl residues. The mineralizing function, if any, of the DHA-rich glycoside is unknown; it could be an intermediate calcium carrier if it also occurs in the calcium-transporting vesicles.

Acknowledgements

Supported by NIH grant AR 36239. The scanning electron micrograph (Fig. 2) was kindly provided by Udayan Parikh.

References

Addadi L, Weiner S (1985) Interactions between acidic proteins and crystals: stereochemical requirements in biomineralization. Proc Natl Acad Sci USA 82: 4110–4114

Blumenkrantz N, Asboe-Hansen G (1973) New method for quantitative determination of uronic acids. Anal Biochem 54: 484–489

Charak JHM, Pirraglia CA, Reithmeier RAF (1990) Interaction of ruthenium red with Ca^{2+}-binding proteins. Anal Biochem 188: 123–131

Crenshaw MA (1972) The soluble matrix from *Mercenaria mercenaria* shell. Biomineralization 6: 6–11

– (1982) Mechanisms of normal biological mineralization of calcium carbonate. In: Nancollas GH (ed) Biological mineralization and demineralization. Springer, Berlin Heidelberg New York, pp 243–357

– Ristedt H (1976) The histochemical localization of reactive groups in septal nacre from *Nautilus pompilius* L. In: Watabe N, Wilbur KM (eds) The mechanisms of mineralization in the invertebrates and plants. University of South Carolina Press, Columbia, SC, pp 355–367

Dimuzio MT, Veis A (1978 a) Phosphophoryns – major noncollagenous proteins of rat incisor dentin. Calcif Tissue Res 25: 169–178

– – (1978 b) The biosynthesis of phosphophoryns and dentin collagen in the continuously erupting rat incisor. J Biol Chem 253: 6845–6852

Domozych DS, Wells B, Shaw PJ (1991) Basket scales of the green alga, *Mesostigma viride*: chemistry and ultrastructure. J Cell Sci 100: 397–407

– – – (1992) Scale biogenesis in the green alga, *Mesostigma viride*. Protoplasma 167: 19–32

Glimcher MJ (1989) Mechanism of calcification: role of collagen fibrils and collagen-phosphoprotein complexes in vitro and in vivo. Anat Rec 224: 139–153

Green MR, Pastewka JV, Peacock AC (1973) Differential staining of phosphoproteins on polyacrylamide gels with a cationic carbocyanine dye. Anal Biochem 56: 43–51

Kyhse-Anderson J (1984) Electroblotting of multiple gels: a simple apparatus without buffer tank for rapid transfer of proteins from polyacrylamide to nitrocellulose. J Biochem Biophys Methods 10: 203–209

Laemmli UK (1970) Cleavage of structural proteins during the assembly of bacteriophage T 4. Nature 227: 680–685

Lee SL, Veis A, Glonek T (1977) Dentin phosphoprotein: an extracellular calcium-binding protein. Biochemistry 16: 2971–2979

Linde A, Lussi A, Crenshaw MA (1989) Mineral induction by immobilized polyanionic proteins. Calcif Tissue Int 44: 286–295

Lyman J, Fleming RH (1940) Composition of sea water. J Marine Sci 3: 134–146

McKee MD, Glimcher MJ, Nanci A (1992) High-resolution immunolocalization of osteopontin and osteocalcin in bone and cartilage during endochondral ossification in the chicken tibia. Anat Rec 234: 479–492

Manton I, Leedale GF (1969) Observations on the microanatomy of *Coccolithus pelagicus* and *Cricosphaera carterae*, with special reference to their origin and nature. J Mar Biol Assoc UK 49: 1–16

– Peterfi LS (1969) Observations on the fine structure of coccoliths, scales, and the protoplast of a freshwater coccolithophorid *Hymenomonas roseola* Stein, with supplementary observations on the protoplast of *Cricosphaera carterae*. Proc R Soc Lond [Biol] 172: 1–15

Marsh ME (1986) Biomineralization in the presence of calcium-binding phosphoprotein particles. J Exp Zool 239: 207–220

– (1989) Self-association of calcium and magnesium complexes of dentin phosphophoryn. Biochemistry 28: 339–345

Sass RL (1983) Calcium-binding phosphoprotein particles in the extrapallial fluid and innermost shell lamella of clams. J Exp Zool 226: 193–203

– – (1984) Phosphoprotein particles: calcium and phosphate binding structures. Biochemistry 23: 1448–1456

– Chang DK, King GC (1992) Isolation and characterization of a novel acidic polysaccharide containing tartrate and glyoxylate residues from the mineralized scales of a unicellular coccolithophorid alga *Pleurochrysis carterae*. J Biol Chem 267: 20507–20512

Milner RE, Famulske KS, Michalak M (1992) Calcium binding proteins in the sarcoplasmic/endoplasmic reticulum of muscle and non-muscle cells. Mol Cell Biochem 112: 1–13

Outka DE, Williams DC (1971) Sequential coccolith morphogenesis in *Hymenomonas carterae*. J Protozool 18: 285–297

Pienaar RN (1969) The fine structure of *Cricosphaera carterae*: I. External morphology. J Cell Sci 4: 561–567

– (1976) The rhythmic production of body covering components in the haptophycean fagellate *Hymenomonas carterae*. In: Watabe N, Wilbur KM (eds) The mechanisms of mineralization in the invertebrates and plants. University of South Carolina Press, Columbia, SC, pp 203–229

Stetler-Stevenson WG, Veis A (1987) Bovine dentin phosphophoryn: calcium ion binding properties of a high molecular weight preparation. Calcif Tissue Int 40: 97–102

Vreeland V (1972) Immunocytochemical localization of the extracellular polysaccharide alginic acid in the brown seaweed, *Fucus distichus*. J Histochem Cytochem 20: 358–367

de Vrind-de Jong EW, Borman AH, Thierry R, Westbroek P, Gruter M, Kamerling JP (1986) Calcification in the coccolithophorids *Emiliania huxleyi* and *Pleurochrysis carterae*: II. Biochemical aspects. In: Leadbeater SC, Riding R (eds) Biomineralization in lower plants and animals. Clarendon Press, Oxford, pp 205–217

van der Wal P, de Jong EW, Westbroek P, de Bruijn WC, Mulder-Stapel AA (1983 a) Polysaccharide localization, coccolith formation and Golgi dynamics in the coccolithophorid *Hymenomonas carterae*. J Ultrastruct Res 85: 139–158

– – – – (1983 b) Calcification in the coccolithophorid alga *Hymenomonas carterae*. In: Hallberg R (ed) Environmental biogeochemistry. Swedish Research Council, Stockholm, pp 251–258 (Ecological bulletin vol 35)

– – – (1983 c) Ultrastructural polysaccharide localization in calcifying and naked cells of the coccolithophorid *Emiliania huxleyi*. Protoplasma 118: 157–168

Westbroek P, van der Wal P, van Emburg PR, de Vrind-de Jong EW, de Bruijn WC (1986) Calcification in the coccolithophorids *Emiliania huxleyi* and *Pleurochrysis carterae*: I. Ultrastructural aspects. In: Leadbeater SC, Riding R (eds) Biomineralization in lower plants and animals. Clarendon Press, Oxford, pp 189–203

Wheeler AP, Sikes CS (1989) Crystal matrix interactions in $CaCO_3$ biomineralization. In: Mann S, Webb J, Williams RJP (eds) Biomineralization – chemical and biochemical perspectives. VCH, New York, pp 95–131